Chapter 5

Case study - application of SBRC to gas reservoir data

5.1 Introduction

The SBRC-method was already applied to several field examples and data sets for different types of reservoirs. Here, one example of the application of SBRC to microseismicity data, which was created during a hydraulic fracturing experiment is shown. Such an example of the applicability of the SBRC approach to data from sedimentary environment is especially interesting for hydrocarbon industry.

5.2 Cotton Valley

In 1997, a fracture imaging study was initiated in the Carthage Cotton Valley Field, Panola County, East Texas (USA). The aim of this study was to determine if microseismicity can be used to accurately map fracture geometry, depict hydraulic fracture design and fracture models (Urbancic et al. [1999]). Furthermore, the optimization of the number and location of wells (reservoir drainage) and the improvement of on-site production methodologies (Walker [1997]) was a main topic. 994 microseismic events with high signal to noise ratio were recorded during the May 14, 1997 Stage 2 fracture treatment in a depth of 2756-2838m in the Carthage Cotton Valley Field (Urbancic et al. [1999]). The following summary is taken from Rutledge and Phillips [2003]:

> *The Carthage Cotton Valley field underlies 1000 km^2 of Panola County, East Texas and is within the northern Gulf of Mexico basin, a structural province of gently dipping beds, open, periclinal folds, and normal faults attributed to diapiric movement of salt. Gas is produced from multiple, low-permeability*

sands within an interbedded sequence of sands and shales. Within the immediate study area, the top of the Cotton Valley formation is about 2600m deep and approximately 325m thick. Overlying the Cotton Valley is the Travis Peak formation, another thick ($\sim$ 450-600m) interval of productive, tight-gas sands interbedded with mudstones. The Cotton Valley and Travis Peak are believed to be within a normal-faulting stress regime with minimum horizontal stress (S_{hmin}) oriented north-northwest. [...] Based on the similarity of expected hydraulic fracture trend and natural fracture orientations, Dutton et al. [1991] noted that Cotton Valley hydraulic-fracture treatments would likely access the natural fracture system.

5.3 Hydraulic fracturing experiment

Injection at the Cotton Valley field took place at a depth of 2756-2838m, where about 1250 m^3 of treated water and viscous gel were injected at approximately constant rate of 40 bpm for about 7 hours as shown in figure 5.1. Microseismicity was observed using downhole seismometers in two monitoring wells located approximately 400m to the east and northeast of the treatment well. The sensor array consisted of 48 three component geophones at 15m spacing in each monitoring well starting at a depth of 2240m (Urbancic et al. [1999]). Only sensors displaying high signal to noise ratios were used to localize the events. Event locations were calculated by employing an iterative joint-hypocenter-velocity inversion approach. Estimates of location error were obtained that ranges from $\pm$14m near the treatment well to $\pm$24m at the wings of western and eastern edges of the fracture zone. The moment magnitudes for the data set ranged from -1.9 to -0.2 with the majority of events having values between -1.2 and -0.9 (Urbancic et al. [1999]).

A total of 994 of 1167 events were located during the injection stages and are used for further analyses. Seismic activity occurred up to 10h after the injection start (see Urbancic et al. [1999]). The event distribution followed an approximately N70E trend from the treatment well, in line with the fracture model design specifications. The events predominantly occurred at two depths within the perforation interval, around 2760m and 2820m.

5.4 Estimation of hydraulic diffusivity

5.4.1 Effective scalar hydraulic diffusivity

The data of the Cotton Valley injection experiment was analysed in terms of the SBRC method. However, the entire experiment was designed as a hydraulic fracturing experiment, the proposed algorithms were applied in order to analyse the spatio-temporal evolution of the seismicity cloud. Furthermore, the philosophy of events being triggered by a diffusive

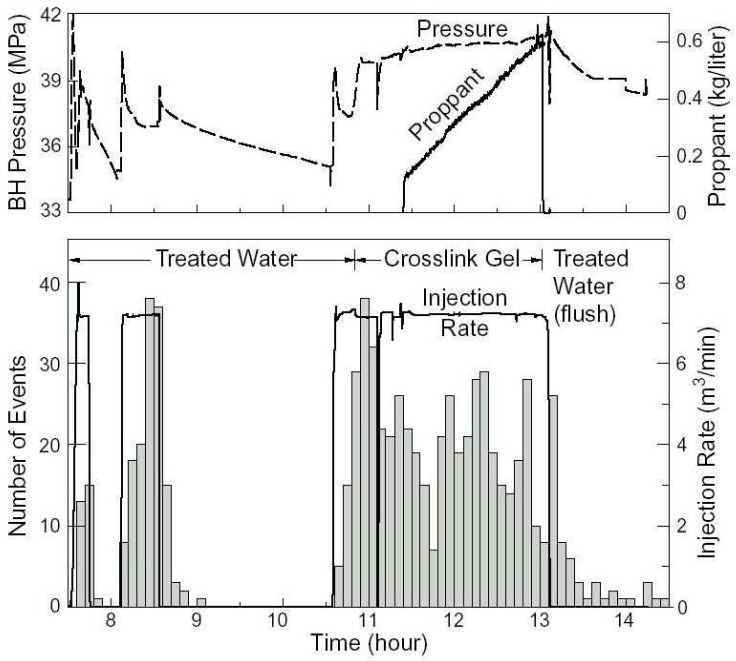

Figure 5.1: Hydraulic fracture treatment data and histogram of the induced microseismic events. BH Pressure is the measured bottom-hole pressure. Taken from Rutledge and Phillips [2003].

process of pore pressure perturbation also in such a case of hydraulic fracturing should be tested. Data was provided by courtesy of Ted Urbancic, Engineering Seismology Group Inc., Canada.

Figure 5.3 shows the spatio-temporal distribution of the Cotton Valley microseismic events together with the estimation of effective scalar hydraulic diffusivity. According to equation (2.6) the distance of each event is plotted versus its occurence time after the beginning of the injection. Good agreement of the spatio-temporal distribution of the events with the predictions using equation (2.6) were found. The diffusivity $D = 0.36m^2/s$ was observed for the seismically-active volume at the depth of 2750-2850 meters.

Several groups of outliers can be observed in figure 5.3, e.g. at times t=0.5h and t=2.5h after the injection. These events occurring early and far away of the injection source point correspond to the events occurring at the tip of the proposed opened fracture. The hypocenters of the events shown in green color above the envelope in figure 5.3 are displayed in figure 5.4. Because these outliers can not be explained by the envelope function according to equation (2.6), it may potentially possible to distinguish between events induced by massive mechanical fracturing and those that are induced due to a diffusive pore-pressure perturbation process by using the SBRC approach.

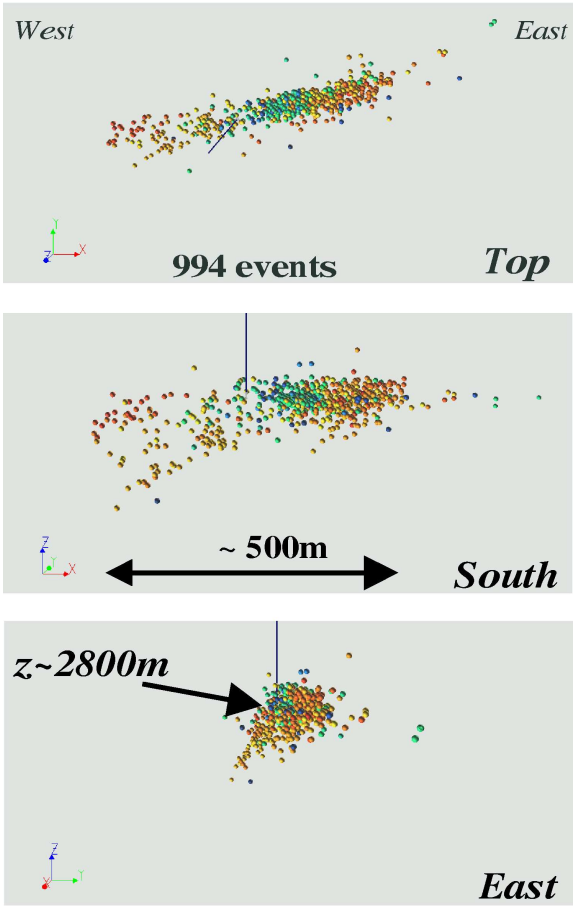

Figure 5.2: The cloud of events from the 1997 injection experiment at the Cotton Valley site (USA) looking from the top, south and east, respectively. The color of the events corresponds to the event occurence time. The injection took place at a depth of 2750-2850m, the total spatial extend in x-direction is approx. 900m. The solid line indicates the borhole.

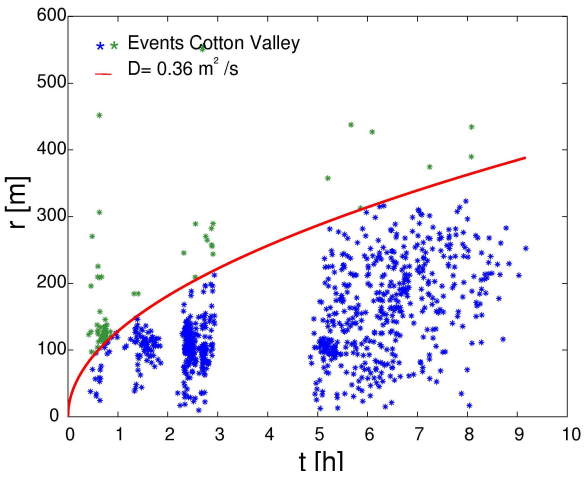

Figure 5.3: Estimation of scalar hydraulic diffusivity at Cotton Valley yielding the estimate $D = 0.36$ m^2/s. Events lying above the fitting envelope are shown in green color.

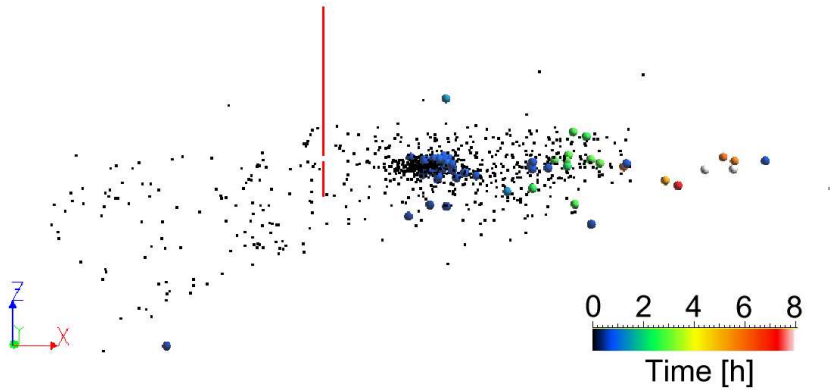

Figure 5.4: Cloud of events of the Cotton Valley injection experiment. Events lying above the fitting envelope corresponding to D=0.36 m^2/s in figure 5.3 (shown in green there) are denoted by large spheres. Colors correspond to the event occurrence time.

5.4.2 Tensor analysis

The Cotton Valley data set was also analysed in terms of 3D properties of hydraulic diffusivity. According to equation (2.9) the event coordinates are transformed into a scaled coordinate system and fitted by an ellipsoid in 3D space using equation (2.10). As mentioned in chapter 2, the half-axes of this tensor are equal to the square roots of the principal diffusivities.

The cloud of events together with the estimation of the tensor of hydraulic diffusivity in the scaled coordinate system is shown in figure 5.5. The fit looks good in all views. The tensor found encloses approximately 94% of the events. The ellipsoid representing the diffusivity tensor in the Cartesian coordinate system together with the cloud of events is shown in figure 5.6. The ellipsoid's maximum half-axis strikes approximately ENE-WSW and dips 10^o. The other two half-axes reveal a strike of NNW-SSE and NW-SE and a dip of 22^o downwards and 66^o upwards, respectively. The exact values are given in table 5.1. The following values were found for the principal diffusivities:

$$\mathbf{D} = \begin{pmatrix} 0.671 & 0 & 0 \\ 0 & 0.015 & 0 \\ 0 & 0 & 0.040 \end{pmatrix} \text{m}^2/\text{s}.$$

The values found agree very well with the value estimated using equation (2.6) for the maximum hydraulic diffusivity which is at least in the same order of magnitude. The mean value of the tensor above is D_{mean}=tr (**D**)/3 = 0.24 m^2/s.

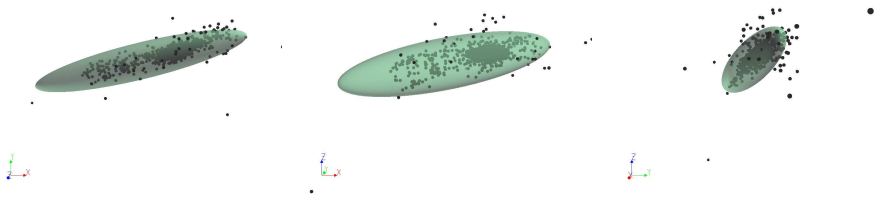

(a) (b) (c)

Figure 5.5: Cloud of events in the scaled coordinate system together with the ellipsoid representing the hydraulic diffusivity tensor looking from the top, south and east, respectively.

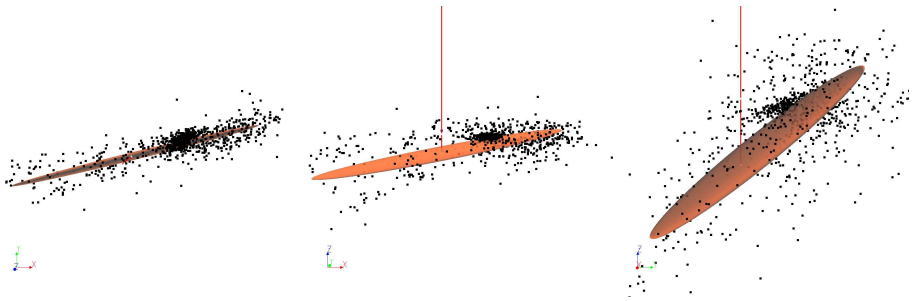

(a) (b) (c)

Figure 5.6: Cloud of events from the Cotton Valley injection experiment in the unscaled coordinate system together with the ellipsoid representing the hydraulic diffusivity tensor looking from the top, south and east, respectively.

	ellipsoid	
	strike	dip
minimum component	N76°	11°
medium component	N350°	-21.6°
maximum component	N321°	65.6°

Table 5.1: Orientations of the principal diffusivities found for the Cotton Valley data set. Negative values of the dip correspond to a vector dipping from the horizontal towards the negative z-axis.

5.4.3 3D reconstruction

If we subdivide the space of the seismically active rock volume at Cotton Valley (figure 5.2) to a number of 3-D cells we are able to define an arrival time of the triggering front into each cell. Of course, some smoothing is required. Such a surface can be constructed for any arrival time presented in microseismic data. Thus, the time evolution of the triggering surface, i.e., the triggering front propagation can be characterized. In a heterogeneous porous medium, the propagation of the triggering front is determined by its heterogeneously distributed velocity. Given the triggering front positions for different arrival times, the 3-D distribution of the propagation velocity can be reconstructed. In turn, the hydraulic diffusivity is directly related to this velocity as explained in chapter 2.

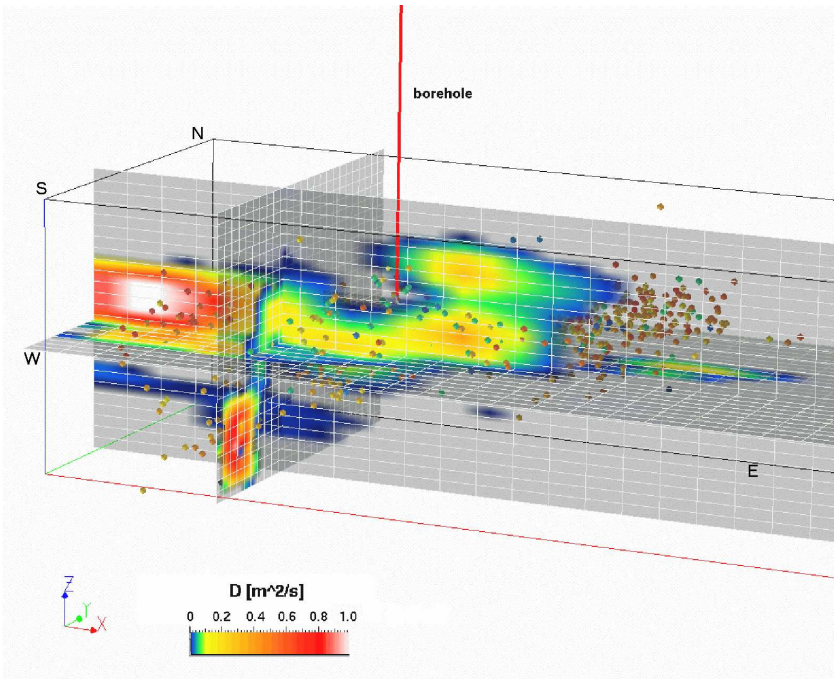

Figure 5.7: 3D-reconstruction of hydraulic diffusivity for Cotton Valley together with the microseismic events. Blue colors indicate low diffusivities, red colors indicate high values. The diffusivity ranges from 0.001 to 1 m^2/s. A high-permeable channel can be identified in the EW-direction (x-direction) from this data set.

Figure 5.7 shows the 3D-reconstruction of hydraulic diffusivity for the Cotton Valley data set using equation (2.34). For the inversion, the isotropic variant of the method was used. A

permeable channel can clearly be identified in the EW-direction from the borhole (yellow and red zones in figure 5.7).